Radiation-induced strengthening and absorption of dislocation loops in ferritic Fe–Cr alloys: the role of Cr segregation

2013 J. Phys.: Condens. Matter 25 265702

(http://iopscience.iop.org/0953-8984/25/26/265702)

IOP PUBLISHING JOURNAL OF PHYSICS: CONDENSED MATTER
J. Phys.: Condens. Matter **25** (2013) 265702 (11pp) doi:10.1088/0953-8984/25/26/265702

Radiation-induced strengthening and absorption of dislocation loops in ferritic Fe–Cr alloys: the role of Cr segregation

D Terentyev[1] **and A Bakaev**[1,2]

[1] SCK·CEN, Nuclear Material Science Institute, Boeretang 200, B-2400 Mol, Belgium
[2] Centre for Molecular Modelling, Ghent University, Technologiepark 903, B-9052 Zwijnaarde, Belgium

E-mail: dterenty@sckcen.be

Received 17 January 2013, in final form 20 May 2013
Published 12 June 2013
Online at stacks.iop.org/JPhysCM/25/265702

Abstract
The understanding of radiation-induced strengthening in ferritic FeCr-based steels remains an essential issue in the assessment of materials for fusion and fission reactors. Both early and recent experimental works on Fe–Cr alloys reveal Cr segregation on radiation-induced nanostructural features (mainly dislocation loops), whose impact on the modification of the mechanical response of the material might be key for explaining quantitatively the radiation-induced strengthening in these alloys. In this work, we use molecular dynamics to study systematically the interaction of dislocations with $1/2\langle 111\rangle$ and $\langle 100\rangle$ loops in all possible orientations, both enriched by Cr atoms and undecorated, for different temperatures, loop sizes and dislocation velocities. The configurations of the enriched loops have been obtained using a non-rigid lattice Monte Carlo method. The study reveals that Cr segregation influences the interaction mechanisms with both $1/2\langle 111\rangle$ and $\langle 100\rangle$ loops. The overall effect of Cr enrichment is to penalize the mobility of intrinsically glissile $1/2\langle 111\rangle$ loops, modifying the reaction mechanisms as a result. The following three most important effects associated with Cr enrichment have been revealed: (i) absence of dynamic drag; (ii) suppression of complete absorption; (iii) enhanced strength of small dislocation loops (2 nm and smaller). Overall the effect of the Cr enrichment is therefore to increase the unpinning stress, so experimentally 'invisible' nanostructural features may also contribute to radiation-induced strengthening. The reasons for the modification of the mechanisms are explained and the impact of the loading conditions is discussed.

(Some figures may appear in colour only in the online journal)

1. Introduction

Dislocation loops are the primary signature of radiation damage in commercial ferritic–martensitic and austenitic steels and model alloys at temperature $\sim(0.3–0.6)T_M$, where T_M is the melting point [1–3]. These defects cause strengthening by obstructing dislocation motion, if the deformation is mediated by dislocation glide. In turn, the obstruction of dislocation motion (strengthening) leads to embrittlement [4], while the ability of dislocations to absorb dislocation loops when unpinning is believed to be the reason for the formation of clear channels [5–7], as suggested by post-deformation investigations. The presence of clear bands, on the other hand, is known to cause plastic flow localization and non-homogeneous deformation, and lead to loss of ductility as a result.

For the above reasons, the dislocation–loop interaction is being intensively studied both experimentally and theoretically. In particular, recently the numerical modelling of this interaction has become a very active field, where two major complementing techniques are applied, namely the discrete dislocation dynamics (DDD; e.g. [8]) and classical molecular dynamics (MD; e.g. [9]) techniques. The direct dislocation–loop interaction involves the atomic rearrangement of dislocation cores and other atomic-scale processes, like the formation of new junctions, their

movement and their unzipping. MD simulations, being inherently atomistic, are especially efficient to use to study dislocation-core effects and defects of nanometric sizes, which are hardly or not at all resolvable in transmission electron microscopy (TEM).

The MD studies performed so far on pure BCC Fe [10] and on FCC Ni [9] and Cu [11] revealed a number of interaction mechanisms resulting in the complete or partial absorption and transformation of dislocation loops. The properties of junctions, or reaction segments (RS), that are formed in the direct dislocation–loop interaction are especially important because they determine the reaction pathway, the unpinning stress and the outcome product [12, 13]. In turn, environmental variables such as temperature and the loading conditions determining the dislocation velocity affect the mobility of the RS and thus indirectly control the interaction mechanism [14, 15].

Real materials (even pure ones) always contain a certain amount of impurities, while alloys contain alloying elements expressly introduced to provide specific properties. These, under irradiation, *a priori* may segregate to lattice imperfections, e.g. dislocation loops, and form so-called 'decorated' loops. By 'decoration', we mean the presence of high concentrations of interstitial impurities or substitutional solute atoms in the strained region around the loop. Recently, the study of the interaction of carbon-decorated $1/2\langle 111\rangle$ loops with dislocations in BCC Fe revealed that the deposition of atoms of this element at the edge of a loop considerably increases the critical stress required for dislocation unpinning [16]. The reasons for the strengthening effect were attributed to the modification of the dislocation–loop interaction mechanism. Importantly, it has been recognized that the modification of the interaction mechanism also applies for small loops (1 nm size, i.e. unresolvable in TEM), thereby making them non-negligible obstacles for dislocations. In contrast, undecorated loops of 1 nm size and below are athermally absorbed on a dislocation line, via flipping [10]. This points to a possible contribution of 'invisible' damage to the net strengthening, which has been suggested to exist at least in ferritic steels [4].

Unlike for pure metals, for concentrated model alloys as well as ferritic–martensitic and austenitic steels, beside the possible decoration with interstitial impurities like C, the segregation of Cr, Ni and other alloying elements is known to occur under irradiation (see e.g. [17]). In particular, the segregation of Cr on both $\langle 100\rangle$ and $1/2\langle 111\rangle$ dislocation loops is a well-established phenomenon, which has been reported by different independent researchers for different grades of Fe–Cr steels and model alloys [18–21]. Recently, an indisputable proof of the segregation of Cr to dislocation lines and dislocation loops was obtained using tomography atom probe (TAP) techniques applied to examine an irradiated high-Cr ferritic–martensitic steel [22]. Hence, it is important to assess the influence of Cr enrichment on the pinning strength of loops and on their ability to be absorbed by moving dislocations.

Here, we perform an atomistic study to investigate the impact of Cr segregation at loops on the interaction with dislocations. In particular, we consider two kinds of interstitial dislocation loops: $1/2\langle 111\rangle$ and $\langle 100\rangle$, which are typically observed under neutron irradiation at elevated temperature in the high-Cr steels and other Fe–Cr model alloys. We put emphasis on the interaction with edge dislocations, since they are known to be more efficient means for loop absorption and removal as compared to screw dislocations. In addition, the contribution to the plastic flow is comparable for edge and screw dislocations at room temperature and above it. We show that Cr enrichment modifies the interaction mechanism for both $1/2\langle 111\rangle$ and $\langle 100\rangle$ loops. We explain the reasons and explore the effect of loop size, test temperature and dislocation velocity on the extra strengthening caused by solute segregation.

2. Computational details

In order to study the equilibrium arrangement of Cr atoms around $1/2\langle 111\rangle$ and $\langle 100\rangle$ dislocation loops, metropolis Monte Carlo (MMC) simulations were used. The case of Fe–9 at.%Cr at 600 K was considered as representative of the Cr contents and irradiation temperatures of technological interest. Then the MMC crystals were embedded in a large MD sample in which the dislocation had been created and relaxed in advance. The crystal was relaxed again, thermalized at the desired temperature, corresponding to the temperature of the mechanical test, and finally loaded to study the interaction of the moving dislocation with the defect of interest.

To describe the Fe–Fe, Fe–Cr and Cr–Cr interactions, we applied the two-band model potential developed in [23], which was extensively exploited in the past few years to model properties of point defects and dislocations, as well as to describe primary damage and phase separation in the Fe–Cr system. The Fe–Fe part of this potential is the one derived by Ackland *et al* in 2004 [24], which is significantly improved compared to previous Fe–Fe many-body potentials, as far as the description of self-interstitial defects and dislocation properties is concerned. Details on MD and MMC tools and studies are provided below.

2.1. MD simulations

To study dislocation–loop interaction we employed the simulation algorithm developed by Osetsky and Bacon [25]. The principal axes x, y and z of the body-centred cubic (BCC) crystal simulation box were oriented along the [111], $[\bar{1}\bar{1}2]$ and $[1\bar{1}0]$ directions, respectively. The initially straight edge dislocation, with $(1\bar{1}0)$ slip plane x–y, was created along the y direction in pure Fe and had Burgers vector (BV) 1/2[111] parallel to the x axis. Periodic boundary conditions were applied along the x and y directions. Along z, the box was divided into three parts: the upper and lower parts consisted of several atomic planes in which atoms were rigidly fixed in their original position relative to each other, whereas atoms in the inner region were free to move during the MD runs. A glide force on the dislocation was generated by displacing the upper rigid block in the x direction, which corresponds to applying simple shear strain e_{xz}. The corresponding

resolved shear stress induced by the applied deformation was calculated as $\sigma_{zx} = F_x/A_{xy}$, where F_x is the total force in the x direction on the lower rigid block due to the atoms in the inner region, and A_{xy} is the xy cross-section area of the box. The size of the inner region of the MD box was 101×3, 30×6 and 25×2 non-equivalent atomic planes along x, y and z (or $25 \times 21 \times 10$ nm^3), respectively. Such crystallites are large enough for considering the interaction of the dislocation with a loop of size up to 5 nm (350 self-interstitial atoms, SIAs), as shown in our previous studies [15, 26, 27]. During an MD run, the dislocation line and dislocation loop were monitored using atomic disregistry analysis, coupled with structural nearest-neighbour analysis (see [12]), as well as by selecting atoms with high potential energy. Statistical averaging was performed over every 250 steps to reveal the atoms belonging to the dislocation core. The latter procedure allowed the identification of the interaction mechanism even at relatively high temperature despite significant thermal noise.

MD simulations were started by initializing the velocity of the relaxed atoms according to Maxwell's distribution for the desired simulation temperature, T, chosen to be in the range of 150–800 K. After thermalization for 10^3 steps, a load was applied at a fixed strain rate. Three different strain rates were applied, resulting in dislocation velocity (v_d) ranging from 4 up to 20 m s^{-1}. Most of the calculations were performed at $v_d = 10$ m s^{-1}. To achieve the desired v_d, the strain rate to be applied, $\dot{\varepsilon}$, was determined according to Orowan's law $\dot{\varepsilon} = pbv_d$, where p is the dislocation density, equal to $1/(L_X \times L_Z)$, and b is the BV. The integration of Newton's equations was performed using a constant time step (2 fs) in the microcanonical *NVE* ensemble, in which number of particles, system volume and total energy are conserved if the work of external forces is taken into account. No temperature control was applied to limit temperature increase during the simulation, as this was negligible in comparison with the simulated temperature. Every interaction geometry has been simulated ten times at each temperature to account for temperature fluctuation effects. The standard errors are reported everywhere with the average values of the unpinning stress.

2.2. MMC simulations

Following our previous work [31, 32], the MMC simulations were done by sampling within the isobaric–isothermal (*NPT*) statistical ensemble, i.e. with number of particles N, pressure P and temperature T being constant. Three kinds of trials were included in the sampling, namely: (i) random displacement of all atoms from their positions (in this trial, lattice relaxation and vibrational entropy are accounted for); (ii) swapping of atoms of different types; (iii) overall change of the volume of the simulation box to maintain the desired pressure. The calculation is stopped once the total energy of the crystal converges to a constant value (with the tolerance of 10^{-3} eV/atom). The MMC sampling was performed in a cubic box of size $8 \times 8 \times 8$ nm^3 containing ~50 000 atoms arranged in a BCC structure, with the principal axes oriented in the same manner as in the MD simulation (see section 2.1), and with an initial random distribution of Cr atoms. The crystals contained interstitial dislocation loops with BV $1/2\langle 111\rangle$ and $\langle 100\rangle$. The former were of circular shape and the latter had square shape with sides oriented along $\langle 001\rangle$ and $\langle 010\rangle$ directions, as found in experiments [33, 34]. Three different sizes were considered for $1/2\langle 111\rangle$ loops, namely 60, 169 and 350 SIAs, which correspond to loop diameters (D_L) of 2, 3.5 and 5 nm, respectively. Only one size of $\langle 100\rangle$ loops was considered, namely 169 SIAs, i.e. slightly above 3 nm. The interstitial dislocation loops of size D_L with BV $= 1/2\langle 111\rangle$ were created by selecting and cutting three circular non-equivalent {111} planes around a desired point in the MMC crystal. Three platelets of $\langle 111\rangle$ crowdions with initial spacing of $0.4 \times a_0$ were introduced there instead and relaxed using the conjugate gradient method.

3. Results

3.1. Local Cr arrangement around dislocation loops

Our previous MMC study, carried out on Fe–10 at.%Cr, showed that both $\langle 100\rangle$ and $1/2\langle 111\rangle$ interstitial dislocation loops of 6 nm diameter exhibit Cr enrichment around their perimeters [31]. The degree of enrichment depends on the simulation temperature and Burgers vector and it appears to be higher for the $\langle 100\rangle$ loop. The degree of enrichment (x_{Cr}) was calculated as the concentration of Cr among the atoms belonging to the edge of the dislocation loop (using structural analysis). It was found that, at 600 K, x_{Cr} is about 25–40 at.%Cr. Here, we considered smaller loops (2–5 nm); however, the results obtained at 600 K for x_{Cr} are close to those in [31], implying that the size of the loop does not significantly influence the enrichment level for the loop density studied. Overall, we could see that x_{Cr} varied from 25 up to 50 at.%Cr. Even though some loose Cr clusters were formed, the composition of Cr in these clusters was too low for considering them as equilibrium α' particles. The Cr decoration was limited to the tensile region of the loop strain field, consistently with the oversized nature of Cr solute atoms in BCC iron. For $1/2\langle 111\rangle$ loops, the enrichment degree was found to increase with loop size. This can be explained by the fact that the sides of relatively small loops do not exhibit fully pronounced dislocation-core structure. Even though, as we already mentioned, there is some variation of x_{Cr} in different loops, we found that statistically (in equivalent MD runs using different initial seeds for velocity distribution) these variations essentially do not affect the average unpinning stress measured in ten runs. Hence, to remain concise we consider only one level of enrichment, 35 at.%Cr.

3.2. Interaction mechanisms with undecorated loops

Before describing the effect of Cr enrichment on the mechanism of interaction between a loop and a moving edge dislocation, it is useful to recall the main features of this mechanism as revealed in pure Fe in our previous studies [10, 12–15, 27]. The average unpinning stress and standard errors are displayed in figures 1(a) and (b) for, respectively, a $\langle 100\rangle$ and a $1/2\langle 111\rangle$ loop interacting with an edge dislocation. All loops

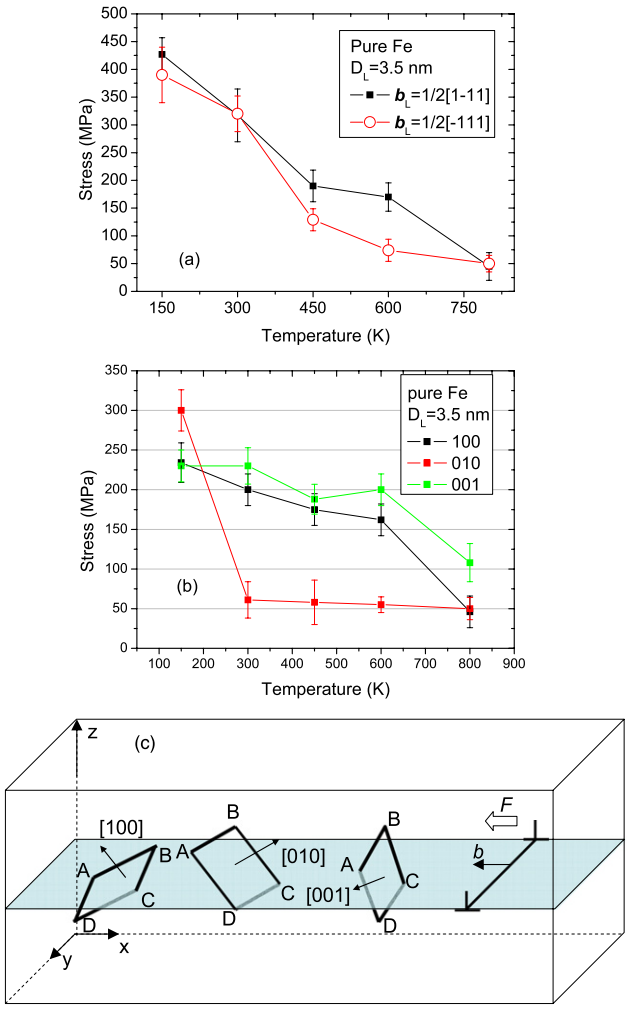

Figure 1. Average unpinning stress calculated in the reactions with (a) $1/2\langle 111\rangle$ and (b) $\langle 100\rangle$ loops, $D_{\mathrm{L}} = 3.5$ nm, undecorated, $v_{\mathrm{D}} = 10$ m s^{-1}. (c) Geometry of interactions considered. The sketch illustrates the orientation and position of the loops before interaction with the positive edge dislocation line moving in a $(\bar{1}10)$ plane in a [111] direction. The square loops have sides along $\langle 100\rangle$ directions and their centres lie on the glide plane. x, y and z in (c) correspond to [111], $[11\bar{2}]$ and $[\bar{1}10]$ crystallographic directions.

considered contained 169 SIAs and their centres were placed at the dislocation glide plane.

In the case of $1/2\langle 111\rangle$ loops, two out of four possible geometries, namely $\boldsymbol{b}_{\mathrm{L}} = 1/2[\bar{1}11]$ and $\boldsymbol{b}_{\mathrm{L}} = 1/2[1\bar{1}1]$, represent the case where the BV is inclined to the dislocation glide plane (DGP). The other two BVs are parallel to the DGP. If the BV of the loop coincides with the BV of the dislocation, the loop is dragged/pulled by the dislocation and it does not enter any direct dislocation reaction. As a result, such interaction causes very little or no resistance to the dislocation glide, because the migration energy of a $1/2\langle 111\rangle$ loop is very small (0.05 eV) so its glide is practically an athermal process [35]. The case of $\boldsymbol{b}_{\mathrm{L}} = 1/2[11\bar{1}]$ and the loop intersecting the glide plane has not been studied so far and we present results here for the first time. The dynamic drag of the loop placed below the DGP was studied already [35] and it was shown that the interaction process is very similar to that for a $1/2[111]$ loop, i.e. an easy glide of the loop together with a dislocation.

Unlike the case of dynamic drag, the strengthening due to the loops with the BVs inclined to the DGP is significant. Here, we recall the basic steps of the interaction mechanisms for two configurations which have already been thoroughly studied in [10, 14, 36].

(a) *Interaction details for* $\boldsymbol{b}_L = 1/2[1\bar{1}1]$: Under the attractive interaction force, the dislocation makes contact with the loop to form an RS of [010] type; the RS, being sessile in the DGP, pins the dislocation, which bows out under increasing stress. The subsequent reaction path depends on temperature and dislocation velocity. At low temperature and high dislocation velocity, a full screw dipole is drawn first and then closes, so the dislocation unpins leaving the partially absorbed $1/2[\bar{1}11]$ loop behind. High temperature and low dislocation velocity conditions favour the glide of the RS over the loop surface, thereby incorporating the loop onto the dislocation line as a double superjog, according to the reaction $1/2[1\bar{1}1]+[010] = 1/2[111]$. The atom-core visualizations of this interaction processes are given, respectively, in figures 7 and 5 from [10].

(b) *Interaction details for* $\boldsymbol{b}_L = 1/2[\bar{1}11]$: Overcoming the initial repulsive interaction, the dislocation makes contact with the loop and an [100] RS is formed; the latter pins the dislocation and, as in the above-described case, the result can be either the complete absorption of the loop or the dipole closure. Even though the mechanism of complete absorption is more involved in this case (see [14, 36] for details), it activates at approximately the same loading conditions as in the case of the loop with $\boldsymbol{b}_{\mathrm{L}} = 1/2[1\bar{1}1]$. This is why the critical shear stresses are similar for the two loops over a wide temperature range.

The interaction with $\langle 100\rangle$ loops is a more involved process and, as follows from figure 1(b), the dependence of the critical stress, τ_{C}, on temperature is rather steep for $\boldsymbol{b}_{\mathrm{L}} = [010]$, while there is a smooth descent for the two other geometries. The reason is the different interaction mechanisms and hence different thermal activation behaviours. Below we describe in more detail the interaction mechanism for each of these of loops and its dependence on temperature, following the earlier study [12] where details and MD snapshots are presented. The sketch of the interaction geometries considered is presented in figure 1(c).

(c) *Interaction details for* $\boldsymbol{b}_L = [100]$: The dislocation line is initially attracted by the loop and forms a $1/2[\bar{1}11]$ segment on contact; this RS pins the dislocation. At low temperature the unpinning requires the formation of a screw dipole, cross-slip of the dislocation arms along the two sides of the loop and finally their closure. The so-called 'bi-loop' formed by a set of [100], $1/2[\bar{1}11]$ and $1/2[111]$ segments is left behind. The visualization of this interaction process is given in figure 6 from [12].

With increasing temperature, an upper segment of [100] loop (segment 'AB' on figure 1(c)) is seen to 'flip' on the glide plane. This 'flip' movement can be interpreted as dissociation of a [100] segment into $1/2[\bar{1}\bar{1}\bar{1}]$ and $1/2[\bar{1}11]$ segments. This reaction is unfavourable and therefore a system must

overcome a certain barrier. This is why such a 'flip' is seen only at high temperature. At intermediate temperatures, the flip occurs rarely and at relatively high applied stress. As a result of this dissociation, the $1/2[\bar{1}\bar{1}\bar{1}]$ segment annihilates with the pre-existing $1/2[111]$ segment, while the $1/2[\bar{1}11]$ segment displaces under the dislocation glide plane. Thus, the remaining lower half of the [100] loop pins the dislocation. With increase of the stress, the [100] segment propagates downwards reacting with the $1/2[\bar{1}11]$ segment and forming a glissile superjog on the dislocation line (in exactly the same manner as in the reaction with a $1/2[\bar{1}11]$ loop).

The flip of an upper loop segment is found to enhance with temperature. Important to note for this interaction geometry is that the flip is not favoured due to the elastic repulsion between an upper segment of a dislocation loop and a dislocation line, while in the configuration with $\boldsymbol{b}_{\mathrm{L}} = [010]$, the same flip movement is favourable because the two segments attract each other.

(d) *Interaction details for* $\boldsymbol{b}_L = [010]$: On the contact with the dislocation, the upper half of the loop changes into the $1/2[1\bar{1}1]$ orientation, and this part immediately slips under the DGP. The lower part of the loop now acts as a lock, which glides across the part with $\boldsymbol{b} = 1/2[1\bar{1}1]$, thereby converting the whole loop into a double superjog with $1/2[111]$ orientation. The last step of the reaction is just the same as in the reaction with a $1/2[1\bar{1}1]$ loop. The details of this process are shown in figure 2 in [12]. The critical stress for a [010] loop is, however, much smaller because the actual size of the loop to be swept by the [010] segment is much larger in the case of the $1/2[1\bar{1}1]$ loop. The difference comes from the fact that $1/2\langle 111\rangle$ loops are freely glissile and therefore adjust the optimum interaction geometry to the approaching dislocation, while $\langle 100\rangle$ loops are immobile (at least in the MD timeframe); therefore its position with respect to the DGP will determine the point of the junction. As a result, the high resistance of the [010] loop is observed only at low temperature, at which the [010] segment has low mobility. Once temperature reaches 300 K and above, the absorption proceeds immediately after the flip, and the critical stress of ∼50 MPa is needed only to accommodate the absorbed loop into a glissile superjog.

(e) *Interaction details for* $\boldsymbol{b}_L = [001]$: The dislocation approaches the loop, and short $1/2[11\bar{1}]$ segments are created at the two corners (lying in the dislocation glide plane; see figure 1(b) from [12]) so the outer arms of the dislocation are pinned at the corners linked by the $1/2[111]$ segment lying across the loop surface. Further load leads to the formation of a screw dipole. In the reaction at 150 K, the loop is finally sheared. In contrast, at $T = 300$ K one of the screw arms double cross-slips (i.e. up and down along 'AD' and 'DC' sides; see figure 1(c)), thereby converting the lower part of the loop into the $1/2[\bar{1}\bar{1}1]$ orientation. The configuration thereby formed is stable and immobile (because of the upper part with [001] orientation). Even though the interaction mechanism changes with temperature, the unpinning of the dislocation still requires the drawing of the screw dipole, and therefore τ_{C} stays nearly constant in the temperature range 150–600 K. At $T = 800$ K, however, the complete absorption of the loop is possible, via the flip of the upper part and via sequential interaction with the $1/2[111]$ and [001] segments of the dislocation and the loop, respectively. One can also see the decrease of the critical stress.

Summing up, one can state that the direct interaction between a dislocation and loop involves the process of formation of mixed segments (following Frank's rule and respecting the conservation of the Burgers vector), the formation of a screw dipole, cross-slip/glide of the screw segments and glide of the reaction segments in the loop habit plane. As discussed in [13], the probability for absorption increases with temperature, since the latter activates the movement of the RS over the loop surface, which is the necessary condition for absorption. Correspondingly, the absorption is the alternative interaction mechanism, which allows the unpinning of the dislocation at lower τ_{C} than in the case of the dipole closure. We now proceed with the detailed description of the interaction of a moving edge dislocation with Cr-enriched loops. In the following subsections, we will consider $\langle 100\rangle$ loops and $1/2\langle 111\rangle$ loops with BVs inclined to DGP and parallel to it.

3.3. The effect of Cr enrichment on the interaction with $\langle 100\rangle$ *loops*

An example of stress–strain loading curves for the [100] loops (both enriched and undecorated) at 150 K and 450 K is shown in figures 2(a) and (b), respectively. We can see that at low temperature the dislocation unpinning from the enriched loop occurs at higher τ_{C}, while at 450 K, there is almost no difference between the two loading curves. In the following we discuss how the enrichment influences the average value of τ_{C} (measured over ten runs at each temperature) and the corresponding unpinning mechanisms.

The resulting average critical stress in the case of the interaction with [001] and [100] loops (of 3.5 nm size) with a dislocation moving at a speed of 10 m s^{-1} is presented in figure 3. We do not present here the results for the [010] orientation, because in this orientation the Cr enrichment does not affect the interaction mechanism and the resolved stress is correspondingly the same, just as in the case of the [001] loop (figure 3(a)). In contrast, we observe a pronounced increase of τ_{C} for the [100] loop when enriched in the temperature range 150–300 K, while at 450 K and higher temperature the strength of the enriched [100] loop is the same as, or lower than, in the undecorated case.

Let us first discuss the reasons for the enhanced strength of the [100] loop seen in the low temperature simulations. The beginning of the interaction occurred in the same manner as in pure Fe, i.e. formation of the RS and screw dipole. However, the cross-slip movement was suppressed on the enriched loop, so that shear occurred at 150 and 300 K. The mechanism becomes identical to that for the undecorated loop at $T = 450$ K and above. This means that, eventually, cross-slip is activated, which is otherwise suppressed due to the enrichment at lower temperature. At high temperature (i.e. above 450 K), undecorated [100] loops flip into the $1/2[\bar{1}11]$ orientation while the pinned dislocation bows out. The flipping is suppressed by Cr decoration, so the enriched

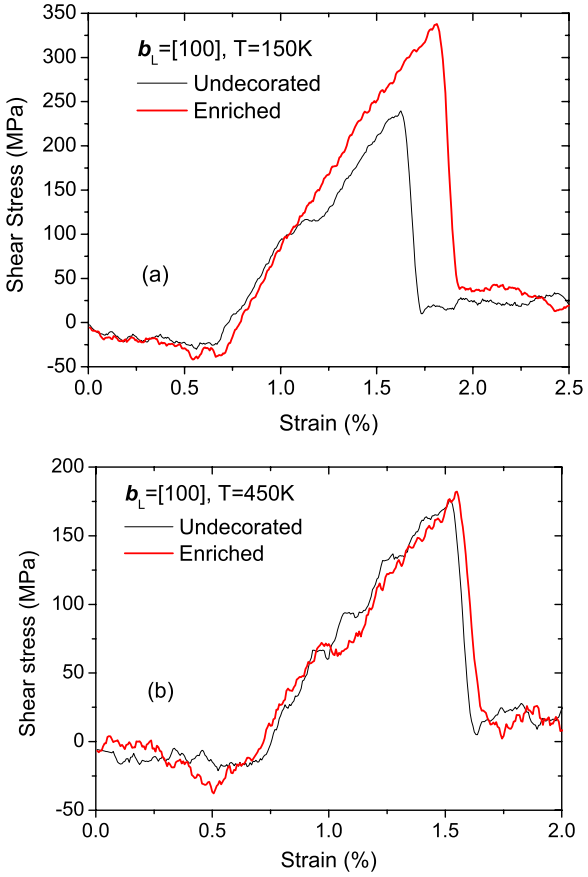

Figure 2. Stress–strain curves computed from MD simulations of the reaction with [100] loops at temperature of (a) 150 and (b) 450 K, $v_D = 10$ m s^{-1}.

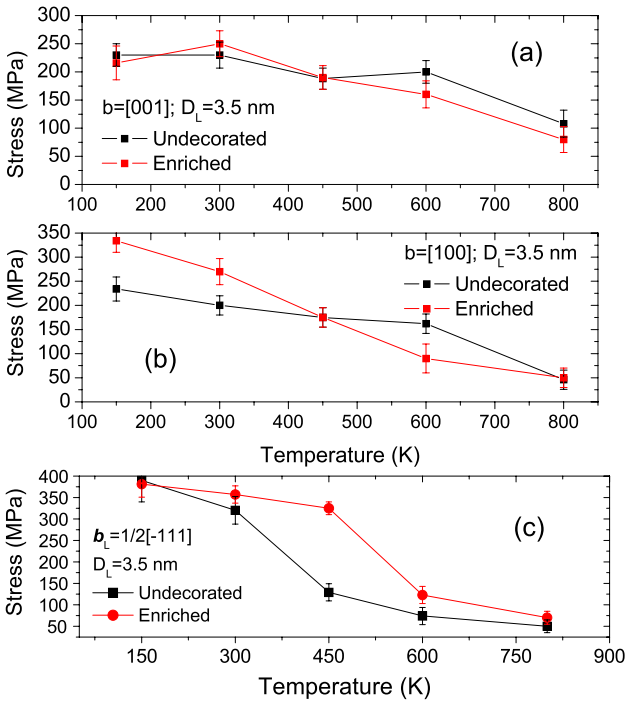

Figure 3. Average unpinning stress calculated in the reactions with (a) [001], (b) [100] and (c) $1/2[\bar{1}11]$ loops, $D_L = 3.5$ nm, $v_D = 10$ m s^{-1}.

loop exhibits the same interaction mechanism as at 450 K, which eventually proceeds at lower stress.

In the case of the [001] loop, there is no effect of Cr enrichment on τ_C; however, the interaction mechanism is affected. As in the case of the [100] loops, Cr enrichment suppresses the cross-slip of the screw dislocation along the loop side in reactions at 150 and 300 K. Yet, since these two mechanisms offer approximately the same loop strength, the $\langle\tau_C\rangle$ values are similar for the decorated and undecorated loops. Above 450 K, thermal activation helped to overcome the resistance of the Cr cloud and the cross-slip mechanism was activated.

The mechanism of interaction with the undecorated [010] loop involved the flip of the upper part into the $1/2[1\bar{1}1]$ orientation on contact with the dislocation line. Apparently, this is energetically a strongly favourable process and it is not suppressed by the enrichment. Once the flip occurs, the upper part slides down leaving the Cr cloud and therefore the enrichment does not play any role in the remaining interaction process.

3.4. The effect of Cr enrichment on the interaction with ⟨111⟩ *loops with BVs inclined to the dislocation glide plane*

The effect of Cr enrichment on the interaction with the 3.5 nm loops with $\boldsymbol{b} = 1/2[\bar{1}11]$ has already been reported in our preliminary study [37]. It was found that the absorption of the loop is suppressed and the corresponding critical stress rises in the temperature range 300–600 K for the dislocation velocity 10 m s^{-1}. The suppression of the absorption reaction by the enrichment was determined to occur due to: (i) freezing of the dislocation loop in its original habit plane, thus delaying the propagation of the [100] reaction segment over the loop surface; and (ii) energetically unfavourable transformation of the $1/2[\bar{1}11]$ into $1/2[111]$ occurring as the [100] RS advances.

The resulting $\langle\tau_C\rangle$ for the $1/2[\bar{1}11]$ is shown in figure 3(c) and the results for the [100] loop containing the same number of defects and loaded in the same conditions are added for comparison. The results for the $1/2[1\bar{1}1]$ and $1/2[\bar{1}11]$ loops are very similar and therefore we do not report or discuss them separately. From figure 3(c), we see that $\langle\tau_C\rangle$ for the enriched loop is substantially higher only at intermediate test temperatures, while it is the same as for the undecorated loop tested at 150 and 800 K. At low temperature this happens because the unpinning proceeds via closure of the screw dipole (for the chosen dislocation velocity) and is therefore not affected by the enrichment. At high temperature, on the other hand, the suppression due to the Cr decoration is overcome with the help of thermal activation.

For the comparison of the effect of the enrichment of $1/2\langle111\rangle$ and $\langle100\rangle$ loops, we selected the [100] loop since this configuration showed the most prominent influence of the enrichment. The comparison given in figure 3 clearly shows that the difference in the interaction mechanisms for the undecorated $1/2[\bar{1}11]$ and [100] loops is also reflected in the case of the enriched loops. In other words: the effect of enrichment appears stronger in the reaction with $1/2\langle111\rangle$ loops than in the case of $\langle100\rangle$ loops. Thus, Cr enrichment

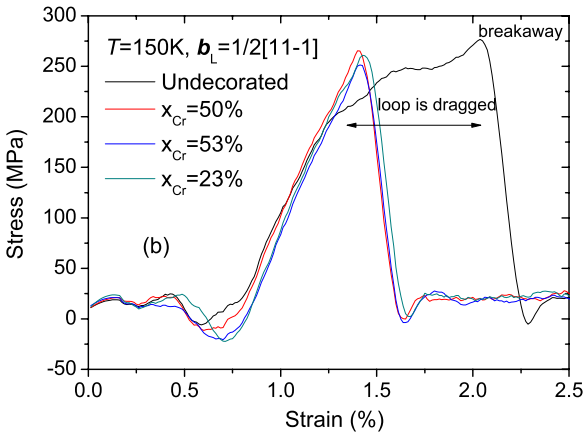

Figure 4. Stress–strain curves computed from MD simulations of the reaction with undecorated and decorated $1/2[11\bar{1}]$ loops, $v_D = 10$ m s^{-1} at $T = 150$ K.

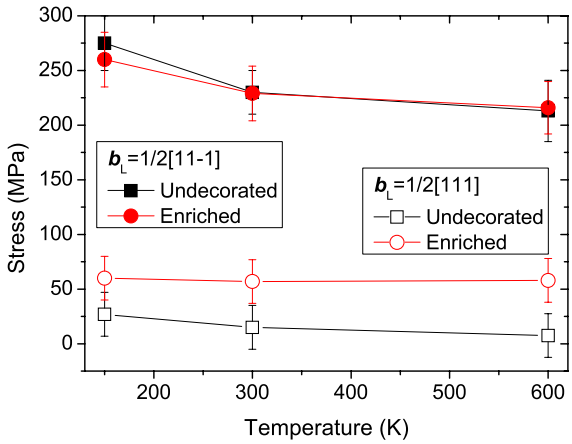

Figure 5. Average unpinning stress calculated in the reactions with $1/2[11\bar{1}]$ and [111] loops, $D_L = 3.5$ nm, $v_D = 10$ m s^{-1}.

is more efficient in the suppression of the propagation of the ⟨100⟩ reaction segment (occurring in reactions with $1/2\langle 111\rangle$ loops) than in the suppression of the cross-slip movement of a screw arm (occurring in reactions with ⟨100⟩ loops).

3.5. The effect of Cr enrichment on the interaction with ⟨111⟩ loops with BVs parallel to the dislocation glide plane

In the case of an undecorated $1/2[111]$ loop, the dislocation does not enter a direct reaction because the 'easily' glissile loop moves away from the approaching dislocation. The steady state flow stress, which is very low for this interaction process, depends mainly on the linear loop density and dislocation velocity and weakly on temperature. The $1/2[11\bar{1}]$ loop is the second possible configuration in which the loop BV is contained in the dislocation glide plane. If the loop does not intersect the glide plane, the dislocation drags or pushes the glissile loop without contact, as reported earlier [35]. The case where the loop intersects the dislocation glide plane has not been studied so far. The details of the interaction process are given in the appendix. Briefly, it is shown that a quadra-point junction is made on the contact and the loop is dragged along the dislocation line via the mechanism involving break-up and reconstruction of this junction. The latter controls the critical stress at which this configuration glides and remains stable. The higher the temperature, the lower the resolved flow stress at which the loop is dragged along the dislocation line. Prior to considering the effect of the enrichment, we recommend the reader to browse the appendix.

Now we move to the description of the effect of Cr enrichment on the interaction with loops having $\boldsymbol{b}_L = 1/2[111]$ and $1/2[11\bar{1}]$. Irrespective of the specific orientation of the loop, the enrichment immobilized the loops (up to the highest temperature studied), causing modification in the interaction mechanisms for both configurations.

In the case of the $1/2[11\bar{1}]$ loop, no dynamic drag was observed along the dislocation line and the dislocation unpinned as soon as the critical stress reached its critical value. Figure 4 shows the corresponding stress–strain curves for the interaction with the undecorated and enriched loops at $v_d = 10$ m s^{-1}: note that in the case of the undecorated loop a limited drag is clearly seen. Even though there is a clear effect of the enrichment on the ability to drag, the critical shear stress for the unpinning is not changed (figure 5), because the unpinning mechanism is not modified at the dislocation velocity studied. If loading tests were performed at lower dislocation velocity, thereby allowing the drag of undecorated loops, one should see an increase of τ_C for the enriched loops.

In the reaction with the enriched $1/2[111]$ loop, the dislocation approached the immobilized loop and cut it in such a way that the lower part of the loop was absorbed by the dislocation line. The details of the process are displayed in figure 6, whose caption describes the basic reaction steps. The overall effect of the enrichment in this case is the increase of τ_C, as shown in figure 5.

Summing up the results presented in this subsection, we note that the Cr enrichment suppresses the glide of a $1/2\langle 111\rangle$ loop and thus suppresses the dynamic loop drag, leading to the modification of the interaction mechanism and overall to an increase of the critical stress.

3.6. The influence of strain rate and loop size on the impact of Cr enrichment

The effect of loop size and dislocation velocity has been separately studied in the case of the $1/2[1\bar{1}1]$ loop, since the Cr enrichment has the strongest effect in the case of $1/2\langle 111\rangle$ loops with the BV inclined to the DGP. Figure 7 displays the added critical stress ($\langle\Delta\tau_C\rangle$) due to the Cr enrichment in the case of dislocation loops containing 60 (1.5 nm), 169 (3.5 nm) and 350 (5 nm) SIAs. For each loop we can see a clearly pronounced maximum corresponding to the temperature at which the influence of the enrichment is the strongest. The temperature corresponding to the maximum $\langle\Delta\tau_C\rangle$ increases with loop size. This originates from the fact that the enrichment enhances τ_C only if the reaction of absorption occurs for the undecorated loop. With increased loop size (and at fixed dislocation velocity), the temperature at which the absorption is triggered also goes up. As a consequence, the peak in figure 7 also shifts towards a higher

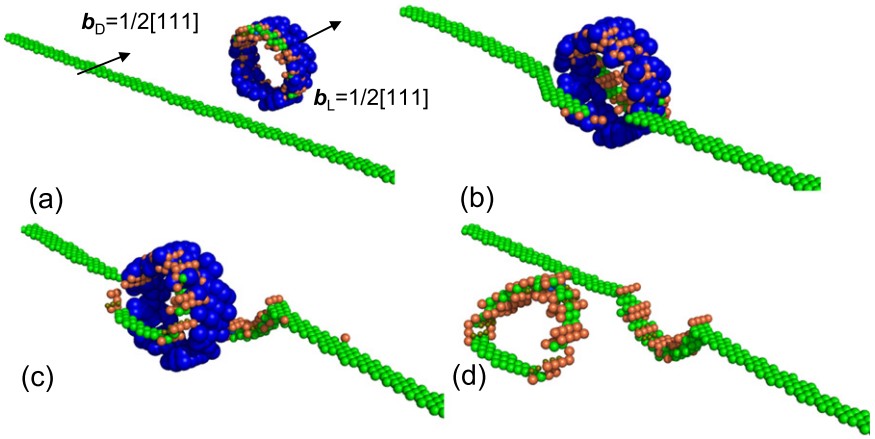

Figure 6. The atom-core visualization of the interaction of the enriched 1/2[111] loop with the dislocation at 150 K and $v_D = 10$ m s^{-1}. Blue balls show Cr atoms which are located in the loop core. (a) The model before load is applied; (b) the dislocation approaches the immobilized loop; (c) the segment substitution has occurred; (d) view of the dislocation-core atoms, showing the half-absorbed loop.

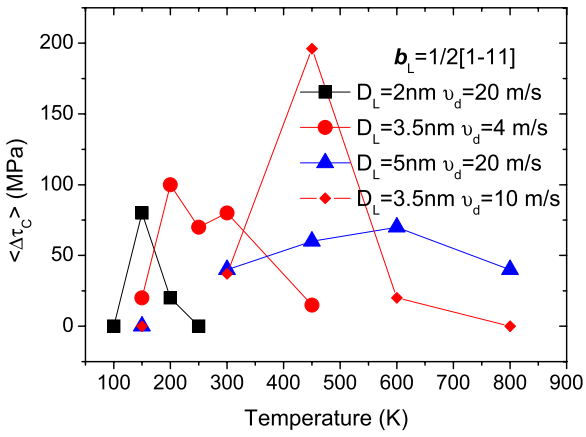

Figure 7. Increase of the average unpinning stress due to the enrichment on the 1/2[1$\bar{1}$1] loop, measured in different loading conditions for different loop sizes as specified in the figure.

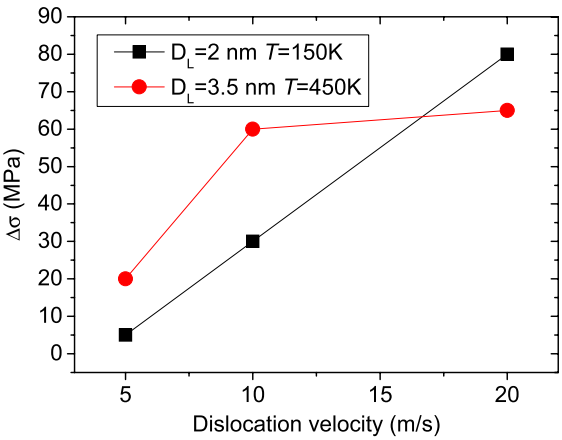

Figure 8. Increase of the average unpinning stress due to the enrichment on the 1/2[1$\bar{1}$1] loop, measured as a function of dislocation velocity for 2 and 3.5 nm loops at two different temperatures, as specified in the figure.

temperature for a larger loop and higher dislocation velocity (see the result for 169-SIA loops in figure 7).

Given that the enhancement of the loop's strength originates from the suppression of the propagation of the RS, one should also expect that the added critical stress $\langle\Delta\tau_C\rangle$ will increase with dislocation velocity (since the RS does not move or moves more slowly, increased dislocation velocity would lead the screw arms to develop more efficiently, so no absorption occurs). To validate this assumption we simulated the interaction process for 60- and 169-SIA loops at 150 K and 450 K respectively, i.e. the temperature at which $\langle\Delta\tau_C\rangle$ is maximum for dislocation velocity of 10 m s^{-1}. The result is presented in figure 8 for dislocation velocity varied from 4 up to 20 m s^{-1}. Indeed, we can see the increase of the loop strength with dislocation velocity confirming our understanding of the mechanism controlling and suppressing the absorption of the loop.

Finally, we note that even small 60-SIA loops now act as non-negligibly strong obstacles at 150 K and above, while in pure Fe the absorption of these and smaller loops is practically athermal in the range of dislocation velocities studied.

3.7. Application of an alternative Fe–Cr interatomic potential

In the present work, we utilized the two-band model Fe–Cr potential developed by Olsson *et al* [23]. An extensive benchmarking of different interatomic potentials for Fe–Cr system, including the one applied here, has been presented recently [28]. The work has shown that the potential applied here provides adequate descriptions of Cr–Cr and Cr–defect interaction. Certainly, the applied potential is no worse than other existing potentials given the problem considered. There is indeed room for further improvement of the potential, as discussed in [29], but at the same time, there is a significant amount of valuable reference data already obtained with the Fe–Fe part of the potential used here [24] regarding the interaction of dislocations with voids, loops and precipitates. Nevertheless, in order to make the statement about the effect of Cr enrichment more robust, we have applied the newly developed Fe–Cr potential [30] for the case of 1/2⟨111⟩ loops. The results are found to be very close to the already presented data showing a strong effect of Cr on the interaction

Table 1. Impact of Cr enrichment on the interaction mechanism and critical resolved shear stress.

Loop orientation	Effect of Cr enrichment	Impact on the reaction outcome	Impact on the critical stress
[001]	Suppression of the cross-slip movement of screw arms of the drawn dipole	Instead of 'bypass' interaction the loop is sheared	Moderate increase
[001]		Shear occurs instead of formation of sessile 'bi-loop'	Minimal
[010]	No change		None
$1/2[\bar{1}11]$ $1/2[1\bar{1}1]$	Suppression of the propagation of reaction segment	Reduction of the absorption, delay of complete absorption to higher test temperature	From moderate to strong increase
$1/2[11\bar{1}]$	Suppression of dynamic drag	None[a]	Minimal
$1/2[111]$		Half of a loop is absorbed	Strong increase

[a] Here, there is no impact on the reaction outcome only if the loading conditions are such that an undecorated loop is not fast enough to be dragged by the dislocation; see the detailed explanation in section 3.5.

mechanism. Given that the paper is already rather lengthy we did not include them in this work.

4. Discussion

Cr enrichment on dislocation loops (of both $\langle 100\rangle$ and $1/2\langle 111\rangle$ types) in Fe–Cr binaries and high-Cr steels has a long experimental story—at least 20 years. Non-equilibrium segregation of Cr to dislocations and dislocation loops was considered as a possible explanation of 'Cr-reduced' swelling as suggested by Little and Stow in 1980 [38], and 'Cr-increased' strengthening suggested by Suganuma in 1983 [39]. Nowadays, fine scale atomic resolution techniques such as TAP [22] give us a proof of the existence of Cr segregation even on very small loops which may be produced directly in collision cascades initiated by heavy ions or neutrons. On the other hand, according to atomistic simulations in Fe or Fe $\sim$ 10%Cr [31] the enrichment of dislocation loops by Cr atoms is energetically favourable, as it corresponds to the redistribution of oversized atoms in the tensile region of edge dislocation lines, in this case prismatic loop edges. In this work, we have studied the impact of this type of decoration on the interaction of the interstitial dislocation loops with an edge dislocation.

The analysis of an extensive number of simulated dislocation–loop reactions (almost one thousand) gave a statistical proof that the Cr enrichment does have an impact on the interaction mechanism, leading to different reaction products and unpinning stresses. Depending on loop type, interaction geometry, temperature and dislocation velocity, the effect of the enrichment may appear stronger or weaker. However, it is clear that the interaction with both $1/2\langle 111\rangle$ and $\langle 100\rangle$ loops is subject to modification if enrichment takes place.

To understand why and how strongly the enrichment changes the interaction process, we have performed simulations with undecorated loops under equivalent loading conditions. By comparing the sequence of the interaction mechanisms we saw that Cr enrichment influences a number of modes of the dislocation movement that occur in the case of undecorated loops. The list of specific effects attributed to the decoration is summarized in table 1. In particular, we would like to highlight the impact of the enrichment on $1/2\langle 111\rangle$ loops, which are practically immobilized by Cr clouds. This causes at least three important modifications in the interaction with dislocations in general (not only edge ones): (i) absence of dynamic drag for loops with BV parallel to DGP; (ii) suppression of the absorption for loops with BV inclined to DGP and (iii) suppression of easy flip of small dislocation loops (2 nm diameter and smaller). When undecorated such loops offer no resistance to dislocation glide.

The effect of Cr enrichment appears in different temperature ranges for $\langle 100\rangle$ and $1/2\langle 111\rangle$ loops because principally different modes of dislocation movement (i.e. glide and cross-slip) are involved in the reactions, depending on the loop type. Hence, the impact of Cr enrichment on the loop strength is expected to play a role in different temperature regimes for $1/2\langle 111\rangle$ and $\langle 100\rangle$ loops. On the basis of the simulations performed here, we can conclude that enrichment will enhance the strength of $\langle 100\rangle$ loops in the low temperature range and of $1/2\langle 111\rangle$ loops in the high temperature range (see example in figure 3). Note that here we have considered only edge dislocations, but for screw dislocations we anticipate that the dynamic drag will also be suppressed for the same reasons as above. This prediction will be validated in our upcoming MD study involving screw dislocations.

Another issue to be discussed is the limited timeframe accessible to MD methods. One needs to explore further the effect of strain rate in the reactions involving the emergence and movement of screw dislocations. This problem is, however, relevant for both undecorated and enriched loops. Indeed, the timeframe for the thermal activation of screw dislocations is totally different from that for edge dislocations. To explore the effect of loading rate, it is necessary to transfer the results obtained here to discrete dislocation dynamics (DDD). In addition, the application of DDD should eventually allow one to explore the net effect of Cr enrichment on the movement of several dislocations in an array of loops, given a specific density and fraction of $\langle 100\rangle$ and $1/2\langle 111\rangle$ loops (to be taken from experiments).

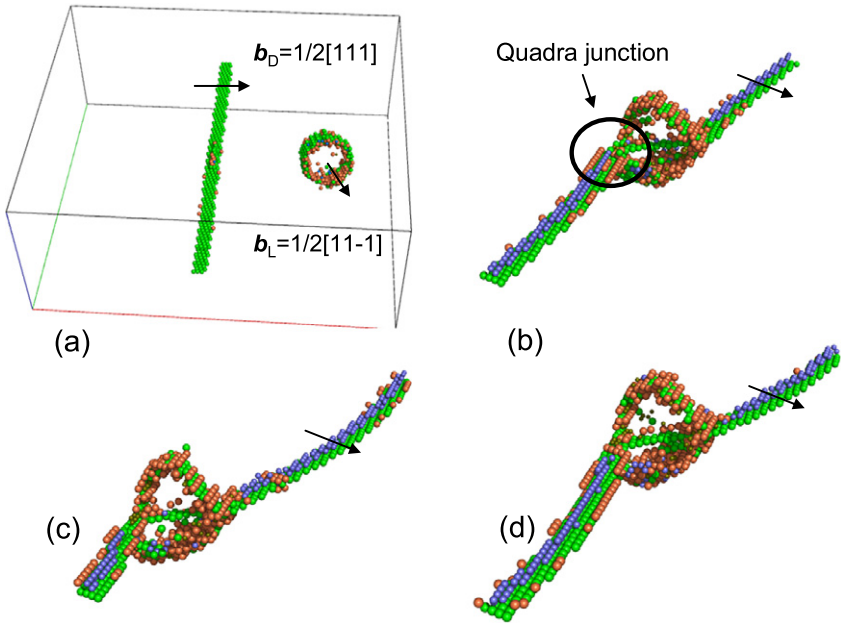

Figure A.1. The atom-core visualization of the interaction of $1/2[11\bar{1}]$ loop ($D_L = 3.5$ nm) with the dislocation at $T = 150$ K and $v_D = 2$ m s^{-1}. (a) The model before the load is applied; (b) formation of two 'quadra-point' junctions, the closest one shown by a circle; (c) the attached loop displaces further along the dislocation line; (d) the attached loop crosses the periodic boundary and keeps moving along the dislocation line.

5. Conclusions

On the basis of the results presented here and accounting for our previously published data [10, 12–15, 27], the following conclusions can be drawn:

(1) The enrichment of Cr on dislocation loops (of both $\langle 100 \rangle$ and $1/2\langle 111 \rangle$ types) and dislocation lines is experimentally observed in concentrated Fe–Cr alloys and high-Cr ferritic steels. According to our atomistic simulations, this enrichment corresponds to the energetically favourable location of oversized Cr atoms in the tensile region of edge dislocation lines. Hence, the Cr enrichment on interstitial dislocation loops can be seen as the decoration of outer loop edges.

(2) Cr enrichment suppresses several modes of dislocation movements which, depending on loading conditions, may lead to the modification of the interaction mechanism with a corresponding change of the unpinning stress (associated with the loop's strength).

(3) We revealed at least three basic effects of the Cr enrichment leading to a strong impact on the interaction mechanism and the loop's strength, by suppressing: (i) cross-slip, (ii) propagation of the reaction segment on the loop surface and (iii) dynamic drag.

(4) The three suppressed mechanisms would generally trigger the removal and transformation (from $1/2\langle 111 \rangle$ to $\langle 100 \rangle$ and vice versa) of the dislocation loops in the course of plastic deformation mediated by dislocations (which is the usual case in ferritic steels). Thus, Cr enrichment suppresses the ability of dislocations to absorb radiation-induced dislocation loops. Moreover, the overall effect of the enrichment is the increase of the obstacle strength of loops.

(5) Cr enrichment enhances especially the strength of small $1/2\langle 111 \rangle$ loops (with $D_L \sim 2$ nm and less, thus being invisible to TEM), which would exhibit negligible resistance to dislocation glide in pure Fe. Hence, 'invisible' matrix damage in combination with local segregation effects may contribute importantly to the net strengthening.

(6) The impact of Cr enrichment on the interaction of dislocations with loops in general diminishes with increasing test temperature, suggesting that it is of thermal activation nature. Hence, the specific impact of the enrichment will depend on at least three parameters: test temperature, dislocation velocity and obstacle spacing.

Acknowledgments

This research was partially supported by the EURATOM seventh Framework Programme, under Grant Agreement No. 212175 (GetMat Project). This work was also partially supported by the European Commission under the Contract of Association between Euratom and the Belgian State, and carried out within the framework of the European Fusion Development Agreement. The authors acknowledge Dr L Malerba for discussion and proofreading. AB acknowledges an FWO grant for financial support.

Appendix. The interaction of an edge dislocation with $1/2[11\bar{1}]$ loops intersecting the glide plane

Consider a series of snapshots showing the interaction of a $1/2[11\bar{1}]$ loop with the edge dislocation, presented in figure A.1(a). The reaction is simulated at 150 K and the dislocation velocity is 2 m s^{-1}. The corresponding

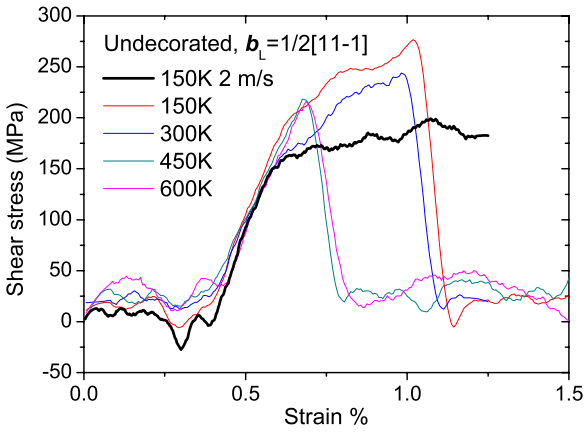

Figure A.2. Stress–strain curves computed from MD simulations of the reaction with $1/2[11\bar{1}]$ loops, $D_L = 3.5$ nm, $v_D = 10$ m s^{-1}, varying temperature, and one curve at 150 K given for $v_D = 2$ m s^{-1}.

stress–strain plot is presented in figure A.2. Initially, there is an attractive interaction and the dislocation approaches the loop. Once the dislocation has reached the loop, it contacts the loop across its surface thus resulting in the formation of a new configuration containing two 'quadra-point' junctions; see figure A.1(b). In principle, this quadra-junction can also be considered as a short [001] segment, which acts as a bridge connecting $1/2[111]$ and $1/2[11\bar{1}]$ segments cutting each other. For some time this complex was stable; however, with increasing stress up to 175–200 MPa it began to move. The configurations of the loop–dislocation complex at strains of 0.75 and 1.25% are shown in figures A.1(c) and (d), respectively. Thus, the loop displaces along the dislocation line while the latter advances. This movement occurs via the mechanism involving break-up and reconstruction of the quadra-point junctions. The latter therefore controls the critical stress at which this configuration glides as a whole. On increasing the dislocation velocity from 2 to 10 m s^{-1}, the loop is not fast enough to follow the dislocation. It starts to curve and, once the critical curvature is reached, the dislocation unpins from the loop at the shear stress of ∼275 MPa. On increasing the test temperature the same breakaway occurs, but at a slightly lower stress. Hence, the ability of the loop to be dragged by the dislocation is determined by the dislocation velocity and linear density of loops, given that we simulate a periodic square array of obstacles.

References

[1] Zinkle S J, Maziasz P J and Stoller R E 1992 Dose dependence of the microstructural evolution in neutron-irradiated austenitic stainless-steel *Workshop on Time Dependence of Radiation Damage Accumulation and its Impact on Materials Properties (Montreux, Switzerland)* p 266

[2] Klueh R L and Harries D L 2001 *ASTM Stock Number: MONO3* ISBN 0-8031-2090-7

[3] Gelles D 2004 *J. Nucl. Mater.* **329–333** 304

[4] Schaeublin R, Gelles D and Victoria M 2002 *J. Nucl. Mater.* **307–311** 197

[5] Fukumoto K, Sugiyama M and Matsui H 2007 *J. Nucl. Mater.* **367–370** 829

[6] Victoria M, Baluc N, Bailat C, Dai Y, Luppo M I, Schaublin R and Singh B N 2000 *J. Nucl. Mater.* **276** 114

[7] Gelles D and Schaeublin R 2001 *Mater. Sci. Eng.* **309–310** 82

[8] Yashiro K, Konishi T and Tomita Y 2008 *Comput. Mater. Sci.* **43** 481

[9] Rodney D 2004 *Acta Mater.* **52** 607

[10] Bacon D, Osetsky Y and Rong Z 2006 *Phil. Mag.* **86** 3921

[11] Nogaret T, Robertson C and Rodney D 2007 *Phil. Mag.* **87** 945

[12] Terentyev D, Grammatikopoulos P, Bacon D and Osetsky Y 2008 *Acta Mater.* **56** 5034

[13] Terentyev D, Osetsky Y N and Bacon D J 2010 *Scr. Mater.* **62** 697

[14] Terentyev D A, Osetsky Y N and Bacon D J 2010 *Acta Mater.* **58** 2477

[15] Terentyev D, Malerba L, Bacon D and Osetsky Y 2007 *J. Phys.: Condens. Matter* **19** 456211

[16] Terentyev D, Anento N and Serra A 2012 *J. Phys.: Condens. Matter* **24** 455402

[17] Takahashi H, Ohnuki S and Takeyama T 1981 *J. Nucl. Mater.* **103/104** 1415

[18] Yoshida N, Yamaguchi A, Muroga T, Miyamoto Y and Kitajia K 1988 *J. Nucl. Mater.* **155–157** 1232

[19] Ohnuki S, Takahashi H and Takeyama T 1981 *J. Nucl. Mater.* **103/104** 1121

[20] Wakai E, Hishinuma A, Usami K, Kato Y, Takaki S and Abiko K 2000 *Mater. Trans. JIM* **41** 1180

[21] Terentyev D, Klimenkov M and Malerba L 2009 *J. Nucl. Mater.* **393** 30

[22] Jiao Z and Was G S 2011 *Acta Mater.* **59** 4467

[23] Olsson P, Wallenius J, Domain C, Nordlund K and Malerba L 2005 *Phys. Rev.* B **72** 214119

[24] Ackland G, Mendelev M, Srolovitz D, Han S and Barashev A 2004 *J. Phys.: Condens. Matter* **16** 1

[25] Osetsky Y N and Bacon D J 2003 *Modelling Simul. Mater. Sci. Eng.* **11** 427

[26] Terentyev D, Bacon D and Osetsky Y 2008 *J. Phys.: Condens. Matter* **20** 445007

[27] Terentyev D, Bacon D J and Osetsky Y N 2010 *Phil. Mag.* **90** 1019

[28] Klaver T P C, Bonny G, Olsson P and Terentyev D 2010 *Modelling Simul. Mater. Sci. Eng.* **18** 075004

[29] Terentyev D, Bonny G, Castin N, Domain C, Malerba L, Olsson P, Moloddtsov V and Pasianot R C 2011 *J. Nucl. Mater.* **409** 167

[30] Terentyev D, Bonny G, Domain C and Pasianot R C 2010 *Phys. Rev.* B **81** 214106

[31] Zhurkin E E, Terentyev D, Hou M, Malerba L and Bonny G 2011 *J. Nucl. Mater.* **417** 1082

[32] Terentyev D, He X, Zhurkin E and Bakaev A 2011 *J. Nucl. Mater.* **408** 161

[33] Masters B 1965 *Phil. Mag.* **11** 881

[34] Jenkins M L, Yao Z, Hernandez-Mayoral M and Kirk M A 2009 *J. Nucl. Mater.* **389** 197

[35] Rong Z, Osetsky Y N and Bacon D J 2005 *Phil. Mag.* **85** 1473

[36] Nomoto A, Soneda N, Takahashi A and Ishino S 2005 *Mater. Trans.* **46** 463

[37] Terentyev D, Bergner F and Osetsky Y O 2013 *Acta Mater.* **61** 1444

[38] Little E and Stow D 1980 *Met. Sci.* 89

[39] Suganuma K and Kayano H 1983 *J. Nucl. Mater.* **118** 234